Chemistry–A European Journal
Research Article
doi.org/10.1002/chem.202403343
Chemistry Europe
European Chemical Societies Publishing
www.chemeurj.org

# Insights into Structural Diversity and Morphotropic Evolution in $A_4Th(WO_4)_4$ (A=Li, Na, K, Rb and Cs) Family

Yi Yu[+],[a] Bin Xiao[+],[b] Rüdiger-A. Eichel,[c] and Evgeny V. Alekseev*[c]

A series of four new thorium tungstates, $A_4Th(WO_4)_4$ (A=Li, K, Rb, Cs), were synthesized using high-temperature solid-state method. Structural studies of the materials reveal distinct structural changes with underlying similarities influenced by the nature of A-site cations. $Li_4Th(WO_4)_4$ exhibits a two-dimensional corrugated sheet structure stabilized by $Li^+$ cations, crystallizing in $P\bar{1}$ space group. $K_4Th(WO_4)_4$ crystallizes in $I4_1/a$ space group and exhibits a three-dimensional framework consisting of $ThO_8$ antiprisms and $WO_4$ tetrahedra. $Rb_4Th(WO_4)_4$ forms in C2/c space group, showcasing a framework with two-dimensional sheet structure. $Cs_4Th(WO_4)_4$ is isostructural to $Rb_4Th(WO_4)_4$ but displays increased interlayer spacing due to the larger ionic radius of Cs. Raman spectroscopy confirms the structural data, revealing distinct vibrational modes that correlate with tungsten coordination changes from $WO_6$ in $Li_4Th(WO_4)_4$ to $WO_4$ in the $Cs_4Th(WO_4)_4$. This study demonstrates how variation of alkali metals affects the structural properties of thorium tungstates series, showing a morphotropic evolution as a factor of the ionic radii of the alkali metals.

## Introduction

In recent decades, the study of actinide compounds has become increasingly important, driven by the need for effective long-term nuclear waste storage solutions and fundamental interest in complex *f*-elements chemistry.[1–8] This growing interest has led to a substantial expansion in our understanding of the structural chemistry of inorganic actinide compounds, encompassing both naturally occurring minerals and synthetic phases.[9–11] For example, one area of particular interest is the complexation of actinyl ions with oxygen-based complexes, involving high-valent elements such as sulfur, chromium, selenium, molybdenum, or tungsten.[12–15] These elements are significant in the context of nuclear waste disposal due to their roles in nuclear engineering and their formation during the burn-up processes of nuclear fuel.[16,17]

Among the various actinide compounds, actinide sulfates, chromates, and selenates are known for their complex and diverse structural chemistries.[18,19] These compounds exhibit fascinating structural features, including cation-cation interactions, microporous frameworks, and the creation of nanotubules.[20,21] The cation-cation interaction in actinyl occurs when an oxygen atom from one actinyl ion serves as an equatorial ligand in a bipyramidal arrangement around another actinyl ion. In other words, one actinyl ion can coordinate with one or several additional actinyl ions. In contrast, actinide molybdates and tungstates tend to adopt structures more akin to dense complex oxides than typical oxo-salts.[22] Uranium molybdates can form limitless structural combinations through corner- and edge-sharing of interpolyhedral linkages, resulting in structures with varying dimensionalities, from simple clusters to complex three-dimensional frameworks.[23,24] This variety in structural forms highlights the complexity and versatility of actinide chemistry.

Tungstates, as well as molybdates, also display a wide range of structural complexities and coordination geometries, offering significant potential for various physical and chemical applications across numerous domains.[22] This structural variety in oxo-tungstates stems from the diverse coordination and arrangements of $WO_x$ (x=4, 5, 6) polyhedra, typically manifesting as $WO_4$ tetrahedra, $WO_6$ octahedra, and $WO_5$ in square pyramids or trigonal bipyramids. The interaction of tungsten with various actinides has led to some novel outcomes.[25,26] Notable among these is $Na_2Li_8[(UO_2)_{11}O_{12}(WO_5)_2]$, a unique compound featuring three distinct uranyl coordination environments.[27] Another example is $Rb_6[(UO_2)_7(WO_5)_2(W_3O_{13})O_2]$, a rare non-molecular inorganic phase with layers containing oxo-tungstate trimers, where tungsten coordinates with four to six oxygen atoms in a distorted tetrahedral and octahedral coordination.[28]

In contrast to uranium phases, the chemistry of thorium tungstates has been less explored. The only well-studied representative in the thorium tungstate family is $Na_4Th(WO_4)_4$, synthesized by using a solid-state method.[29] Th can serve as a surrogate for $An^{4+}$ (such as U/Np/Pu) in term of their crystal chemical and structural behaviour in different inorganic systems.[29] Usage of Th can help in avoiding challenges and costs associated with chemical studies of transuranic elements,

[a] *Y. Yu*[+]
*School of Physics and Electronics Information, Gannan Normal University, Ganzhou 341000, PR China*
[b] *B. Xiao*[+]
*Institute of Energy and Climate Research (IEK-6), Forschungszentrum Jülich, D-52428 Jülich, Germany*
[c] *R.-A. Eichel, E. V. Alekseev*
*Institute of Energy Technologies (IET-1), Forschungszentrum Jülich GmbH, Jülich, Germany*
*E-mail: e.alekseev@fz-juelich.de*
[+] *These authors contributed equally to this work.*

**Table 1.** Crystallographic data for $Li_4Th(WO_4)_4$, $Na_4Th(WO_4)_4$, $K_4Th(WO_4)_4$, $Rb_4Th(WO_4)_4$ and, $Cs_4Th(WO_4)_4$, respectively.

| Compound | $Li_4Th(WO_4)_4$ | $K_4Th(WO_4)_4$ | $Rb_4Th(WO_4)_4$ | $Cs_4Th(WO_4)_4$ |
|---|---|---|---|---|
| Dimension | 2D | 3D | 2D | 2D |
| Mass | 1135.336 | 1287.696 | 1473.172 | 1662.924 |
| Space group | $P\bar{1}$ | I41/a | *C2/c* | *C2/c* |
| a (Å) | 7.6361(3) | 11.6590(16) | 26.933(2) | 27.9211(16) |
| b (Å) | 7.9631(3) | 11.6590(16) | 6.4055(4) | 6.6392(3) |
| c (Å) | 10.0568(3) | 13.029(3) | 11.4186(11) | 11.5061(5) |
| α (deg) | 81.116(3) | 90 | 90 | 90 |
| β (deg) | 81.524(3) | 90 | 113.828(9) | 114.270(5) |
| γ (deg) | 78.966(3) | 90 | 90 | 90 |
| V (Å$^3$) | 588.62(4) | 1771.1(6) | 1802.0(3) | 1944.42(18) |
| Z | 2 | 4 | 4 | 4 |
| λ(Å) | 0.71073 | 0.71073 | 0.71073 | 0.71073 |
| F(000) | 1052.0 | 2360.0 | 2648.0 | 2936.0 |
| μ(cm$^{-1}$) | 51.622 | 35.259 | 44.466 | 38.642 |
| $\rho_{calcd}$ (g cm$^{-3}$) | 7.059 | 5.175 | 5.770 | 5.995 |
| R(F) for $F_o^2 > 2\sigma(F_o^2)$[a] | 0.0302 | 0.0288 | 0.0780 | 0.0383 |
| $wR_2$ ($F_o^2$)[b] | 0.0800 | 0.0580 | 0.1987 | 0.0926 |

[a] $R(F) = \Sigma||F_0| - |F_c||/\Sigma|F_0|$. [b] $R(F_0^2) = [\Sigma w(F_0^2 - F_c^2)^2/\Sigma w(F_0^4)]^{1/2}$.

but it has to be noted that Th is not a full chemical analogue of other actinides and only can serve as a model for their structural behaviour in 4+ oxidation state.

To address the gap in Th–W–O system, our recent studies have focused on thorium tungstates with alkaline cations, taking inspiration from the successes in the actinide molybdate family. As part of these efforts, we report the synthesis, crystal structure, and characterization of four new thorium tungstates with general compositions of $A_4Th(WO_4)_4$ (A=Li, K, Rb and Cs).

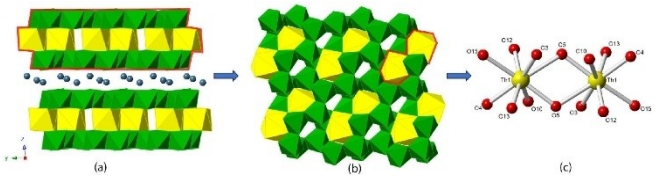


**Figure 1.** View of crystal structure $Li_4Th(WO_4)_4$. (a) layered sheets (b) a single layer (c) local structural geometry.

## Results and Discussion

### Structural Studies

#### *$Li_4Th(WO_4)_4$*

$Li_4Th(WO_4)_4$ crystallizes in $P\bar{1}c$ space group, and its cell parameters were presented in Table 1.

The structure features a two-dimensional corrugated sheets with $[Th(WO_4)_4]^{4-}$ composition. The $Li^+$ cations are located between the sheets and serve to balance the negative charge of the sheets, as illustrated in Figure 1(a). This arrangement, with interconnected anionic sheets and charge-compensating cations in the interlayers, is typical for thorium-based minerals and synthetic compounds.[30,31]

$Li_4Th(WO_4)_4$ contains one distinctive W-site and four Th-sites. Each W atom forms a slightly distorted $WO_6$ octahedral configuration that interconnected to create zigzag chains with $[WO_4]^{2-}$ composition, as depicted in Figure 1(b). The W–O bond lengths in these chains are in the range from 1.77(2) Å to 2.34(4) Å, which is typical for tungsten oxides.[32] Each Th atom is coordinated by eight oxygen atoms forming $ThO_8$ bicapped trigonal prismatic arrangements. These groups are further interconnected into the $Th_2O_{14}$ dimers. These dimers are located between the $[WO_4]^{2-}$ chains, contributing to the corrugated sheet structure presented in Figure 1(c). The Th–O bond distances within these $Th_2O_{14}$ units vary from 2.29(9) Å to 2.64(3) Å, indicating a complex atomic interaction, but still falls in the normal range of Th–O distance.[33]

The higher density of $Li_4Th(WO_4)_4$, compared to other compounds from $A_4Th(WO_4)_4$ family, is primarily attributed to the coordination geometry of W atoms and the significantly smaller size of the $Li^+$ cation. In $Li_4Th(WO_4)_4$, tungsten adopts a distorted $WO_6$ octahedral coordination, which allows for a more compact, edge-sharing arrangement (Figure 1(b)) of the structural units. This octahedral configuration facilitates closer packing, enhancing the overall density of the material. In contrast, compounds like $K_4Th(WO_4)_4$, $Rb_4Th(WO_4)_4$, and $Cs_4Th(WO_4)_4$ involve a transition to the single, non-polymerized $WO_4$ tetrahedral coordination, resulting in less efficient packing and lower overall density due to the larger volumes occupied by the

tetrahedra. Furthermore, the small size of the $Li^+$ cation enables it to fit more effectively between the anionic layers, further reduces interlayer spacing and contributes to a dense crystal structure.

### $K_4Th(WO_4)_4$

$K_4Th(WO_4)_4$, is isostructural with $Na_4Th(WO_4)_4$,[29] and crystallizes in $I4_1/a$ space group with unite cell parameters given in Table 1. This structure is based on the $[Th(WO_4)_4]^{4-}$ framework fragments, consisting of $ThO_8$ antiprisms and $WO_4$ tetrahedra, as shown in Figure 2. The Th–O bond lengths in $K_4Th(WO_4)_4$ are in the range from 2.39(5) Å to 2.46(5) Å. $K_4Th(WO_4)_4$ belongs to the larger $A_4An(MO_4)_4$ group (where A=Na, K; An=Th, U, Pu; M=Mo, W), known for their characteristic scheelite superlattice structures.[34]

We perform a comprehensive analysis of An–O bond lengths across all phases within this group. Figure 3 demonstrates the local coordination environments of actinide ions and

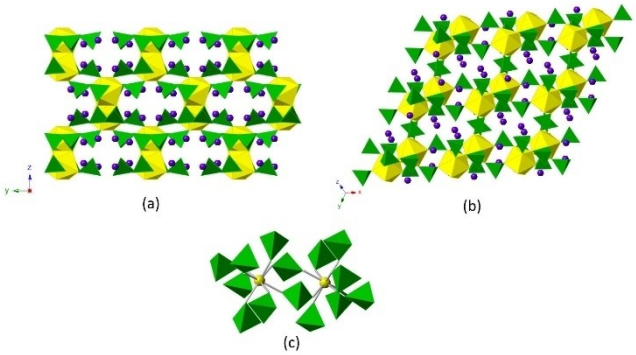


**Figure 2.** View of crystal structure $K_4Th(WO_4)_4$. (a) 3D framework observed along c-axis. (b) along [111] direction. (c) local coordination for Th and W.

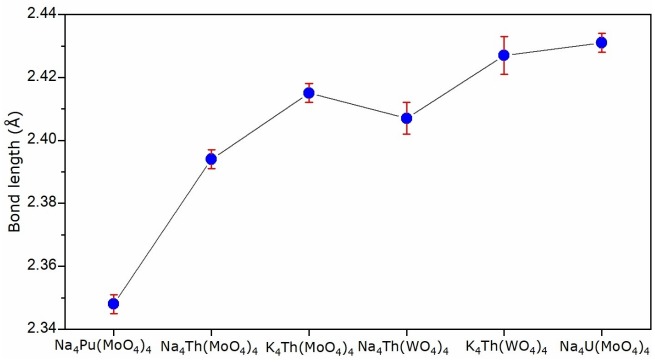


**Figure 3.** Average An–O bond lengths in the $A_4An(MO_4)_4$ series (A=Na, K; An=Th, U, Pu; M=Mo, W).

their corresponding An–O bond lengths in compounds of $Na_4Pu(MoO_4)_4$,[35] $Na_4Th(MoO_4)_4$,[35] $K_4Th(MoO_4)_4$,[36] $Na_4Th(WO_4)_4$,[29] $K_4Th(WO_4)_4$, and $Na_4U(MoO_4)_4$,[37] respectively. Their average An–O bond lengths are summarized in Table 2.

We focus on examining the impact of the actinide element's nature, the presence of molybdenum or tungstate, and the type of alkali element on the An–O bond length. Starting with $Na_4Pu(MoO_4)_4$, it has the shortest average An–O bond length of 2.348(3) Å, this can be attributed to the smaller ionic radius of Pu compared to that of Th and U, so called actinide contraction. It leads to a denser electron cloud around the plutonium ion, resulting in shorter bond lengths. In contrast, $Na_4Th(MoO_4)_4$ and $K_4Th(MoO_4)_4$, which contain thorium, show longer bond lengths of 2.400(3) Å and 2.415(3) Å, respectively.

The increase in bond length in $K_4Th(MoO_4)_4$ compared to $Na_4Th(MoO_4)_4$ can be mainly ascribed to the stronger electronegativity of Na than that of K. This make it is easier for oxygen to accept the electrons from K then from Na and no need to be closer to Th to compensate it. Additionally, the compounds containing $WO_4$, namely $Na_4Th(WO_4)_4$ and $K_4Th(WO_4)_4$, exhibit even longer Th–O bond lengths: 2.407(5) Å and 2.427(6) Å, respectively. This elongation is also predominantly because of difference in electronegativity of Na and K, as aforementioned. In addition, the structural differences between the $MoO_4$ and $WO_4$ groups, including bond angles and electron cloud distribution, further contribute to the variations observed in bond lengths across these compounds.

Uranium containing $Na_4U(MoO_4)_4$, has the longest average An–O bond length (2.431(3) Å) in the whole family. The elongation of the U–O bond length in $Na_4U(MoO_4)_4$ is influenced by the large ionic radius of uranium. Uranium, as one of the largest actinides, naturally forms longer bonds.[38] The polarizability of uranium also interacts with the oxygen atoms in the $MoO_4$ group, contributing to longer and weaker bonds.[38]

It has to be noted that the bond distances in these isostructural actinide compounds closely align with those in the scheelite structure of $CaWO_4$.[39] This uniformity points to the underlying crystal chemical stability of the scheelite-related structures, for the variety of the $An^{4+}$ elements in the presence of Na and K cations.

### $Rb_4Th(WO_4)_4$

$Rb_4Th(WO_4)_4$ crystallizes in C2/c (Table 1) and features a layered structure as it is shown on the Figure 4(a). The layers have $[Th(WO_4)_4]^{4-}$ composition, where each thorium atom is in the center of a $ThO_8$ square anti-prism, surrounded by eight $WO_4$ tetrahedra via vertices sharing. A notable aspect of this

**Table 2.** Comparison of average An–O (An=U, Th and Pu) bond lengths in phases isostructural with $K_4Th(WO4)_4$.

| | $Na_4Pu(MoO_4)_4$ | $Na_4Th(MoO_4)_4$ | $K_4Th(MoO_4)_4$ | $Na_4Th(WO_4)_4$ | $K_4Th(WO_4)_4$ | $Na_4U(MoO_4)_4$ |
|---|---|---|---|---|---|---|
| An–O | 2.348(3) | 2.400(3) | 2.415(3) | 2.407(5) | 2.427(6) | 2.431(3) |
| ref. | [35] | [35] | [37] | [29] | This work | [37] |

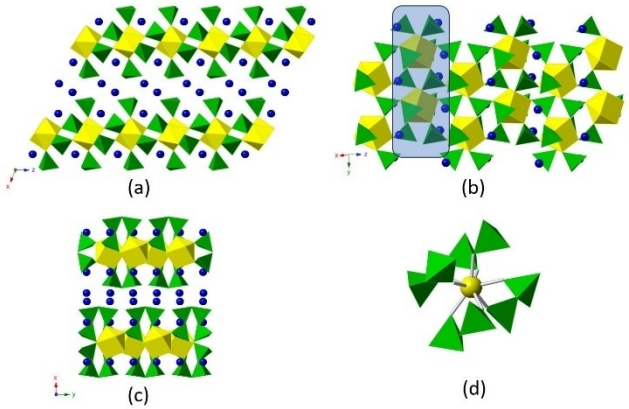


**Figure 4.** View of crystal structure $Rb_4Th(WO_4)_4$. (a) 2D sheets observed along [010] direction. (b) a single layer with the highlighted building chain (c) 2D sheets observed along [001] direction. (d) the local coordination environment for Th.

structure, highlighted in Figure 4(b), is the presence of individual thorium tungstate chains within the described 2D layers. These chains are composed of $ThO_8$ square anti-prisms linked by two $WO_4$ tetrahedra and they align side-by-side along the [010] axis, creating the two-dimensional sheets, portrayed in Figure 4(c). The Rb(2) cations are positioned within the sheets, while the Rb(1) cations serve to crosslink neighboring layers, which stack parallel to the c-axis (Figure 4(d)).

As shown in Figure 5(a) and (b), the building blocks inside the $Rb_4Th(WO_4)_4$ layers demonstrate some similarity to those found in the $A_4Th(WO_4)_4$ (A=Na, K) series, but are different with respect to geometry. $Rb_4Th(WO_4)_4$ features one crystallographically independent Th site and two W sites, in contrast to the single Th and W sites found in the $K_4Th(WO_4)_4$. The mean bond length of Th–O in $Rb_4Th(WO_4)_4$~2.407 Å, which is shorter than the 2.427 Å bond length found in $K_4Th(WO_4)_4$.The topological differences between the $Rb_4Th(WO_4)_4$ sheets and the $A_4Th(WO_4)_4$ (A=Na, K) frameworks are demonstrated in Figure 5(c) and (d), using a black-and-white schematic representation. In this depiction, black nodes represent $ThO_8$ square anti-prisms, and white nodes symbolize $WO_4$ tetrahedra. In both structures, all black vertices (Th sites) are 8-connected. However, in $A_4Th(WO_4)_4$, each W site is 2-connected, whereas in $Rb_4Th(WO_4)_4$, half of the W sites are 3-connected, and the remaining are 1-connected. This results in $Th[(WO_4)_4]^{4-}$ chains forming a three-dimensional framework in $A_4Th(WO_4)_4$, as opposed to the layered structure in $Rb_4Th(WO_4)_4$.

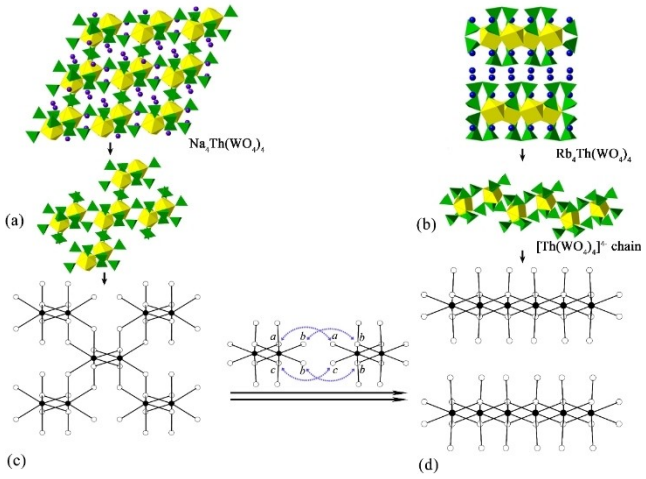


**Figure 5.** Topological transformation between crystal structure of $Na_4Th(WO_4)_4$ and $Rb_4Th(WO_4)_4$. (a) view structure of $Na_4Th(WO_4)_4$ (b) view structure of Rb4Th(WO4)$_4$ (c, d) black-and-white representation shows the topological transformation from 3D framework to 1D chain.

The transformation from a three-dimensional framework to two-dimensional sheets can be conceptualized through a 'cutting and gluing' procedure, involving the reconfiguration of the local coordination of W sites. Initially, the W–O connections at the edge of each $Th[(WO_4)_4]^{4-}$ fragment in the $A_4Th(WO_4)_4$ framework are severed to isolate individual $Th[(WO_4)_4]^{4-}$ chains. The corresponding W points on the side of each chain are labeled with letters a, b, c, d, as shown in Figure 5. The transformation to a two-dimensional sheet structure is completed by joining corresponding white nodes (a–a, b–b, c–c, d–d). This process alters the coordination number of W atoms without modifying the fundamental topology of the $Th[(WO_4)_4]^{4-}$ chains, illustrating the flexible nature of Th–O–W linkages and their ability to form different structural arrangements with similar basic units.

### *$Cs_4Th(WO_4)_4$*

$Cs_4Th(WO_4)_4$ crystallizes in the monoclinic P2/c space group. Geometrically, this compound is isostructural with $Rb_4Th(WO_4)_4$. However, a significant difference arises due to the larger ionic radius of the $Cs^+$ cation, which is 1.74 Å, compared to the 1.61 Å of $Rb^+$ cations.[40] This difference in ionic radius leads to an increase of interlayer distance in $Cs_4Th(WO_4)_4$, (12.72(6) Å compared to an interlayer distance found in $Rb_4Th(WO_4)_4$ 12.31(5) Å, measured as Th–Th distance between neighbouring layers). The lengths of the Th–O bonds vary between 2.34(5) Å to 2.46(3) Å, with the average value of 2.41(5) Å. This average Th–O bond length is slightly shorter compared to the 2.42(5) Å observed in the Rb analogue. Meanwhile, the W–O bond lengths span between 1.71(3) Å and 1.82(5) Å. These bond distances are found to be comparable with those observed in the structurally similar $Rb_4Th(WO_4)_4$.

### Morphotropic Evolution in the $A_4Th(WO_4)_4$ (A=Li, Na, K, Rb, and Cs) Series

The series of thorium tungstates $A_4Th(WO_4)_4$ (where A=Li, Na, K, Rb, and Cs) indicates a morphotropic evolution driven by the substitution of alkali metal ions, and reflects a systematic structural transformation across the series. One can select three distinctive structural types within the series. Beginning with $Li_4Th(WO_4)_4$, the structure is characterized by compact, two-dimensional corrugated sheets stabilized by the small ionic radius of $Li^+$ ions, facilitating tight layering and efficient space

utilization within the crystal lattice. As we look on the Na and K analogs, there is a notable shift towards a more open, three-dimensional scheelite superlattice structure, indicative of a morphotropic phase boundary influenced by the increasing ionic radius of the substituting alkali metals. This structural evolution is further exemplified by Rb/$Cs_4Th(WO_4)_4$ members, where the larger $Rb^+$/$Cs^+$ ions promote the formation of new two-dimensional thorium tungstate sheets, diverging from the dense packing observed in the lithium-based compound towards a more layered arrangement. However, sheets in Rb/Cs phases are less dense than those in Li analogs and leave enough space for Rb/Cs cations to be settled within the sheets. It has been noted that, throughout these morphotropic evolutions, the coordination of Th remains constant with $ThO_8$ polyhedra, while W transitions from $WO_6$ octahedra in the Li member to $WO_4$ tetrahedra coordination in the other phases. This consistency in Th coordination amidst the structural transformations underscores the stability of $ThO_8$ polyhedra, even as the surrounding lattice undergoes significant structural changes.

A similar morphotropic evolution has been observed in the $A_2Th(AsO_4)_2$ series, where A also represents by Li, Na, K, Rb, and Cs.[41] Starting with $Li_2Th(AsO_4)_2$ that features a 2D layered, monoclinic structure, a significant morphotropic boundary is observed transitioning to $Na_2Th(AsO_4)_2$, which forms in an open 3D framework within an orthorhombic space group to accommodate larger ionic size of Na. This morphotropic evolution continues from $Na_2Th(AsO_4)_2$ to the isostructural $K_2Th(AsO_4)_2$ and $Rb_2Th(AsO_4)_2$, and ultimately reaches the most open structure of $Cs_2Th(AsO_4)_2$. Similar to $Na_2Th(AsO_4)_2$, each of these compounds crystallizes in a 3D framework, reflecting structural adjustments in response to the increasing ionic radii of the alkali metals.

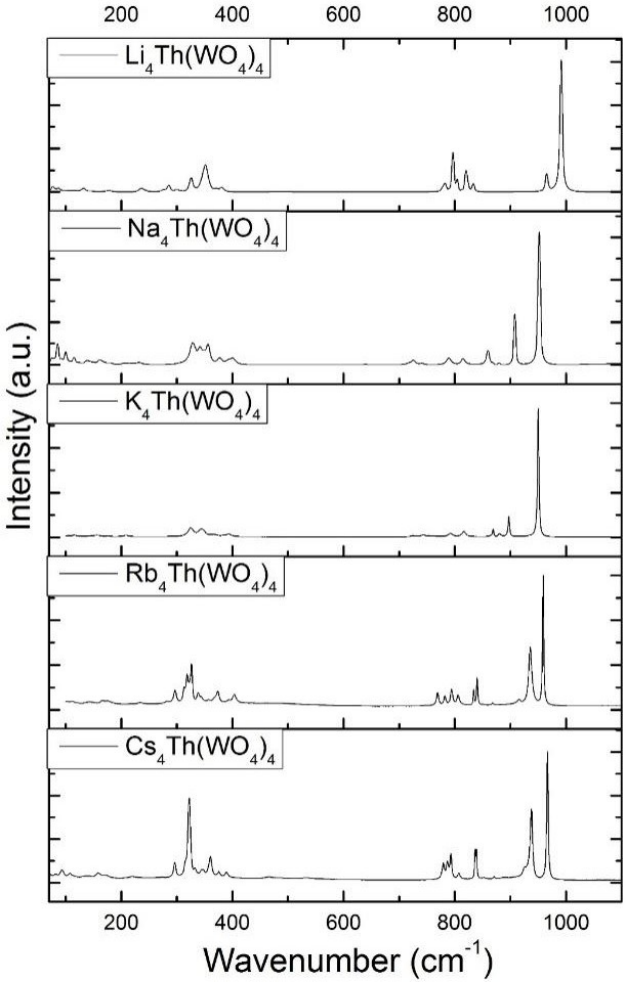


**Figure 6.** Raman spectra for compounds $A_4Th(WO_4)_4$ (A=Li, Na, K, Rb and Cs) are recorded from 100 $cm^{-1}$ to 1100 $cm^{-1}$.

### Raman Analysis

Raman spectroscopy was utilized to study the vibrational properties of the $A_4Th(WO_4)_4$ series, where A=Li, Na, K, Rb, and Cs. This analysis covered a spectral range from 100 $cm^{-1}$ to 1100 $cm^{-1}$, as depicted in Figure 6.

The study categorized the vibrational behaviors of these compounds into two main frequency ranges: low-frequency vibrations (100 to 250 $cm^{-1}$), which are attributed to the movements of the lattice structure, and high-frequency vibrations (250 to 1100 $cm^{-1}$), which are related to the behavior of tungstate ions. The $[WO_4]^{2-}$ anion exhibits two types of vibrational modes: internal modes, in which the anion's center of mass does not move, and external modes, in which the anion acts as a rigid body.[42] In aqueous solutions, the isolated $[WO_4]^{2-}$ anion forms a tetrahedral shape with $T_d$ symmetry, displaying four primary internal vibrational modes.[43] However, in the solid state, within the crystal structures of $A_4Th(WO_4)_4$ (where A=Na, K, Rb, and Cs), the interactions between $[WO_4]^{2-}$ anions and the vibrational modes of the cations ($Na^+$, $Rb^+$, $K^+$, and $Th^{4+}$) lead to the distortion of the $WO_4$'s local symmetry and this subsequently causes the broadening and splitting of these modes.

In the case of $Li_4Th(WO_4)_4$, the presence of six $WO_6$ octahedra, each with $C_1$ site symmetry, results in a Raman spectrum that different from other compounds in this series. This compound exhibits a high-frequency peak at 990(1) $cm^{-1}$, which is attributed to the symmetric stretching mode ($v_1$) of the W–O bonds in the $WO_6$ octahedra.[44,45] The factor group analysis predicts a vibrational mode distribution of $\Gamma_{acoustic} = 3A_u$ and $\Gamma_{optic} = 75A_g + 72A_u$, indicating a complex interaction of optical modes that likely contributes to the distinct spectral features observed.[46,47] This is in contrast to the $Na_4Th(WO_4)_4$ and $K_4Th(WO_4)_4$ compounds, where a single $WO_4$ group with $C_1$ site symmetry leads to a highest peak at 950(1) $cm^{-1}$, associated with the W–O in $WO_4$ tetrahedra,[48,49] suggesting a simpler tungsten coordination and a closer structural similarity between these two compounds. Furthermore, examining the $Rb_4Th(WO_4)_4$ and $Cs_4Th(WO_4)_4$ compounds, both of which contain two $WO_4$ groups with identical $C_1$ site symmetry, reveals a similar pattern in their Raman spectra with the highest peaks at 960(1) $cm^{-1}$ and 963(1) $cm^{-1}$, respectively. These peaks denote the stretching mode ($v_1$) of W–O in the $WO_4$ tetrahedra. The

vibrational mode distributions for these compounds, as indicated by $\Gamma acoustic = A_u + 2B_u$ and $\Gamma optic = 37A_g + 36A_u + 38B_g + 36B_u$, suggest a more complex optical mode interaction compared to the Na and K compounds. The broadening and splitting of vibrational modes across a range of 400 $cm^{-1}$ to 960 $cm^{-1}$ in these compounds can be attributed to the interactions between the $[WO_4]^{2-}$ anions and the various cations,[50,51] which also cause a slight shift in peak positions compared to $Na_4Th(WO_4)_4$ and $K_4Th(WO_4)_4$.

## Conclusions

In this study we explore a novel family of thorium tungstates, namely $A_4Th(WO_4)_4$ (A=Li, Na, K, Rb, and Cs). It highlights how the change in nature of alkali metal ions can significantly influence the structural properties of these compounds, demonstrating a clear correlation between the ionic radius of the alkali metals and the resulting crystal structures. From the compact two-dimensional sheets in $Li_4Th(WO_4)_4$ to the more expansive $Na_4Th(WO_4)_4$ and $K_4Th(WO_4)_4$, and further to less dense two-dimensional sheets in $Rb_4Th(WO_4)_4$ and $Cs_4Th(WO_4)_4$, the study illustrates a systematic morphotropic transitions within the series. The average bond lengths analyzed across various compounds isostructural to $K_4Th(WO_4)_4$, ranging from $Na_4U(MoO_4)_4$ to $Na_4Pu(MoO_4)_4$, demonstrates a consistent geometrical configuration akin to the scheelite structure of $CaWO_4$. Notably, the shortest bond length in $Na_4Pu(MoO_4)_4$ reflects plutonium's smaller ionic radius, while the longer lengths in thorium and uranium compounds are influenced by their larger ionic radii and the substitution of tungsten for molybdenum. This consistency and variation underline the influence of ionic size and elemental composition on the structural characteristics of these actinide compounds. Raman spectroscopy analysis of the $A_4Th(WO_4)_4$ series (A=Li, Na, K, Rb, Cs) provides additional insights into the vibrational properties affected by various cation substitutions. The spectral variations, especially between $Li_4Th(WO_4)_4$ and other compounds, highlight the structural differences and their influence on tungsten coordination.

## Experimental Section

### Crystal Syntheses

For all syntheses, analytical grade $Th(NO_3)_4 \cdot 5H_2O$ (Merck), $WO_3$ (Alfa-Aesar), and $ANO_3$ (A=Li, Na, K, Rb, and Cs) were utilized directly as received, without any additional purification. For each compound $A_4Th(WO_4)_4$ (A=Li, K, Rb, and Cs), the molar ratios of Th:W:A were maintained at 1:1:1. The synthesis method was consistent across these samples; therefore, to avoid repetition, $Li_4Th(WO_4)_4$ will be discussed as a representative example. In a typical synthesis, for example, a homogeneous mixture was prepared by grinding 0.1 g of thorium nitrate hydrate ($Th(NO_3)_4(H_2O)_5$), 0.0124 g $LiNO_3$ and 0.4169 g of tungsten trioxide ($WO_3$) using an agate mortar and pestle until a fine, uniform powder was achieved. This mixture was then carefully transferred to a clean platinum crucible for heat treatment. The loaded crucible was placed in a high-temperature CARBOLITE CWF 1300 furnace. The furnace temperature was ramped up to 1323 K and maintained at this level for a duration of 6 hours to ensure complete reaction. Following the high-temperature treatment, the furnace was programmed to cool at a controlled rate of 5 K/h down to a temperature of 1023 K. Once the lower temperature threshold was reached, the crucible was removed from the furnace and the materials were rapidly quenched to room temperature to keep the quality of the crystals. This quenching process was critical in preserving the quality of the formed crystals. The final product was a composite of $A_4Th(WO_4)_4$ crystals embedded within a matrix of glassy mass. However, due to the overlapping morphological features of the crystals and the glass pieces, distinguishing between the two for yield quantification proved to be challenging.

### Crystallographic Studies

The crystals of obtained thorium molybdates selected for data collection were mounted on glass fibers and then aligned on an Agilent SuperNova (Dual Source) diffractometer. All data were collected using monochromatic Mo-K$\alpha$ radiation with an incident wavelength of 0.71073 Å and a beam size of approximately 30 μm in diameter. More than a hemisphere of data was collected for each crystal, and the three-dimensional data were reduced and outliers identified using the software CrysAlisPro. Data were corrected for Lorentz polarization, absorption and background effects. The SHELXL program was used for the determination and refinement of the structures.[52] The structures of the $A_4Th(WO_4)_4$ series were solved by direct methods and their crystallographic information is given in Table 1($Li_4Th(WO_4)_4$–CCDC: 2349856), $K_4Th(WO_4)_4$–CCDC: 2349857, $Rb_4Th(WO_4)_4$–CCDC: 2349858, and $Cs_4Th(WO_4)_4$–CCDC: 2349859.

### Raman Spectroscopy

Unpolarized Raman spectra were recorded with a Horiba LabRAM HR spectrometer using a Peltier cooled multi-channel CCD detector. An objective with a 50x magnification was linked to the spectrometer, allowing the analysis of samples as small as 2 μm in diameter. All the samples were in the form of single crystals. The incident radiation was produced by a He–Ne laser at a power of 17 mW ($\lambda = 632.81$ nm). The focal length of the spectrometer was 800 mm and 1800 gr/mm grating was used. The spectral resolution was around 1 $cm^{-1}$ with a slit of 100 μm. The spectra were recorded in the range of 100 $cm^{-1}$–4000 $cm^{-1}$. No photoluminescence was observed.

## Acknowledgements

EVA, is grateful for the funding within AL1527/3-1 project. YY is supported with the National Natural Science Foundation of China (12264004), the Natural Science Foundation of Jiangxi Province (20202ACBL214020). Open Access funding enabled and organized by Projekt DEAL.

## Conflict of Interests

The authors declare no conflict of interest.

## Data Availability Statement

The data that support the findings of this study are available from the corresponding author upon reasonable request.

**Keywords:** Thorium · Tungstates · Morphotropic · Alkali cations · Structure

[1] M. Altmaier, X. Gaona, T. Fanghänel, *Chem. Rev.* **2013**, *113*, 901–943.
[2] R. M. Pallares, R. J. Abergel, *Nanoscale* **2020**, *12*, 1339–1348.
[3] L. C. Motta, J. Autschbach, *Nat. Commun.* **2023**, *14*, 4307.
[4] K. A. Pace, V. V. Klepov, A. A. Berseneva, H. C. Z. Loye, *Chem-Eur. J.* **2021**, *27*, 5835–5841.
[5] G. L. Murphy, P. Kegler, E. V. Alekseev, *Dalton Trans.* **2022**, *51*, 7401–7415.
[6] Z. R. Jones, M. Y. Livshits, F. D. White, E. Dalodière, M. G. Ferrier, L. M. Lilley, K. E. Knope, S. A. Kozimor, V. Mocko, B. L. Scott, B. W. Stein, J. N. Wacker, D. H. Woen, *Chem. Sci.* **2021**, *12*, 5638–5654.
[7] K. Lv, S. Fichter, M. Gu, J. März, M. Schmidt, *Coordin. Chem. Rev.* **2021**, *446*, 214011.
[8] K. Li, W. Liu, H. L. Zhang, L. W. Cheng, Y. G. Zhang, Y. X. Wang, N. Chen, C. Q. Zhu, Z. F. Chai, S. A. Wang, *Radiochim. Acta* **2023**, *111*, 1–42.
[9] J. B. Lu, D. C. Cantu, C. Q. Xu, M. T. Nguyen, H. S. Hu, V. A. Glezakou, R. Rousseau, J. Li, *J. Chem. Theory Comput.* **2021**, *17*, 3360–3371.
[10] G. J. P. Deblonde, M. Zavarin, A. B. Kersting, *Coordin. Chem. Rev.* **2021**, *446*, 214130.
[11] R. Kloditz, S. Fichter, S. Kaufmann, T. S. Brunner, P. Kaden, M. Patzschke, T. Stumpf, P. W. Roesky, M. Schmidt, J. März, *Inorg. Chem.* **2020**, *59*, 15670–15680.
[12] B. Xiao, P. Kegler, D. Bosbach, E. V. Alekseev, *Inorg. Chem.* **2016**, *55*, 4626–4635.
[13] B. Xiao, P. Kegler, T. M. Gesing, L. Robben, A. Blanca-Romero, P. M. Kowalski, Y. Li, V. Klepov, D. Bosbach, E. V. Alekseev, *Chem.-Eur. J.* **2015**, *22*, 946–958.
[14] B. Xiao, P. Kegler, D. Bosbach, E. V. Alekseev, *Dalton Trans.* **2016**, *45*, 15225–15235.
[15] J. M. Berg, A. J. Gaunt, I. May, A. L. Pugmire, S. D. Reilly, B. L. Scott, M. P. Wilkerson, *Inorg. Chem.* **2015**, *54*, 4192–4199.
[16] S. J. Morrison, P. S. Mushovic, P. L. Niesen, *Environ. Sci. Technol.* **2006**, *40*, 2018–2024.
[17] J. R. Muscatello, D. M. Janz, *Sci. Total Environ.* **2009**, *407*, 1318–1325.
[18] B. Xiao, E. Langer, J. Dellen, H. Schlenz, D. Bosbach, E. V. Suleimanov, E. V. Alekseev, *Inorg. Chem.* **2015**, *54*, 3022–3030.
[19] B. Xiao, J. Dellen, H. Schlenz, D. Bosbach, E. V. Suleimanov, E. V. Alekseev, *Cryst. Growth Des.* **2014**, *14*, 2677–2684.
[20] S. V. Krivovichev, P. C. Burns, I. G. Tananaev, B. F. Myasoedov, *J. Alloy Compd.* **2007**, *444–445*, 457–463.
[21] S. V. Krivovichev, V. Kahlenberg, I. G. Tananaev, R. Kaindl, E. Mersdorf, B. F. Myasoedov, *J. Am. Chem. Soc.* **2005**, *127*, 1072–1073.
[22] B. Xiao, T. M. Gesing, P. Kegler, G. Modolo, D. Bosbach, H. Schlenz, E. V. Suleimanov, E. V. Alekseev, *Inorg. Chem.* **2014**, *53*, 3088–3098.
[23] T. Nagai, N. Sato, S. Kitawaki, A. Uehara, T. Fujii, H. Yamana, M. Myochin, *J. Nucl. Mater.* **2013**, *433*, 397–403.
[24] M. Keskar, S. K. Sali, N. D. Dahale, K. Krishnan, R. Phatak, N. K. Kulkarni, S. Kannan, *J. Nucl. Mater.* **2012**, *421*, 147–152.
[25] M. Dufaye, S. Duval, T. Loiseau, *CrystEngComm* **2020**, *22*, 3549–3562.
[26] M. T. Galante, A. Živković, J. C. Alvim, C. C. C. Kleiner, M. Sangali, S. F. R. Taylor, A. J. Greer, C. Ardacre, K. Rajeshwar, R. Caram, R. Bertazzoli, R. T. Macaluso, N. H. de Leeuw, C. Longo, *ACS Appl. Mater. Interfaces* **2021**, *13*, 32865–32875.
[27] E. V. Alekseev, S. V. Krivovichev, W. Depmeier, O. I. Siidra, K. Knorr, E. V. Suleimanov, E. V. Chuprunov, *Angew. Chem., Int. Ed.* **2006**, *118*, 7391–7393.
[28] A. N. Seliverstov, E. V. Suleimanov, E. V. Chuprunov, N. V. Somov, E. M. Zhuchkova, M. I. Lelet, K. B. Rozov, W. Depmeier, S. V. Krivovicheve, E. V. Alekseev, *Dalton Trans.* **2012**, *41*, 8512–8514.
[29] G. B. Jin, L. Soderholm, *J. Solid State Chem.* **2011**, *184*, 337–342.
[30] R. M. Hazen, R. C. Ewing, D. A. Sverjensky, *Am. Mineral.* **2009**, *94*, 1293–1311.
[31] J. Blundy, B. Wood, *Rev. Minera. Geochem.* **2003**, *52*, 59–123.
[32] I. Z. Hager, R. El-Mallawany, M. Poulain, *J. Mater. Sci.* **1999**, *34*, 5163–5168.
[33] C. D. Tutson, A. E. V. Gorden, *Coordin. Chem. Rev.* **2017**, *333*, 27–43.
[34] M. Pagès, W. Freundlich, *J. Inorg. Nucl. Chem.* **1972**, *34*, 2797–2801.
[35] N. D. Dahale, M. Keskar, K. D. S. Mudher, *J. Alloy Compd.* **2006**, *415*, 244–250.
[36] M. Huyghe, M. R. Lee, M. Quarton, F. Robert, *Acta Crystallogr. C.* **1991**, *47*, 1797–1799.
[37] N. D. Dahale, M. Keskar, N. K. Kulkarni, K. D. S. Mudher, *J. Alloy Compd.* **2007**, *440*, 145–149.
[38] S. C. Bart, K. Meyer, *Struct. Bonding* **2008**, *127*, 119–176.
[39] M. I. Kay, B. C. Frazer, I. Almodovar, *J. Chem. Phys.* **1964**, *40*, 504–506.
[40] R. D. Shannon, C. T. Prewitt, *Acta Cryst.* **1970**, *B26*, 1046–1048.
[41] N. Yu, V. V. Klepov, G. Modolo, D. Bosbach, E. V. Suleimanov, T. M. Gesing, L. Robben, E. V. Alekseev, *Inorg. Chem.* **2014**, *53*, 11231–11241.
[42] M. Crane, R. L. Frost, P. A. Williams, J. T. Kloprogge, *J. Raman Spectrosc.* **2002**, *33*(1), 62–66.
[43] F. D. Hardcastle, I. E. Wachs, *J. Raman Spectrosc.* **1995**, *26*(6), 397–405.
[44] M. Picquart, S. Castro-Garcia, J. Livage, C. Julien, E. Haro-Poniatowski, *J. Sol-Gel Sci. Technol.* **2020**, *18*, 199–206.
[45] A. Kania, A. Niewiadomski, G. E. Kugel, *Phase Transit.* **2013**, *86*, 290–300.
[46] L. J. Burcham, I. E. Wachs, *Spectrochim. Acta, Part A* **1998**, *54*, 1355–1368.
[47] L. Macalik, J. Hanuza, A. A. Kaminskii, *J. Mol. Struct.* **2000**, *555*, 289–297.
[48] K. Subbotin, P. Loiko, S. Slimi, A. Volokitina, A. Titov, D. Lis, E. Chernova, S. Kuznetsov, R. M. Solé, U. Griebner, V. Petrov, M. Aguiló, F. Díaz, P. Camy, E. Zharikov, X. Mateos, *J. Lumin.* **2020**, *228*, 117601.
[49] Q. Zhang, L. L. Xu, X. L. Tang, F. Y. Huang, X. H. Wu, Y. X. Li, Y. L. Jing, Z. K. Han, H. Su, *J. Alloy Compd.* **2021**, *874*, 159928.
[50] Y. Peng, K. Z. Li, J. H. Li, *Appl. Catal., B* **2013**, *140–141*, 483–492.
[51] M. Maczka, M. Ptak, K. Hermanowicz, A. Majchrowski, A. Pikul, J. Hanuza, *Phys. Rev. B* **2011**, *83*, 174439.
[52] G. M. Sheldrick, *Acta Crystallogr. C* **2015**, *71*, 3–8.

Manuscript received: September 6, 2024
Accepted manuscript online: December 2, 2024
Version of record online: December 10, 2024